Screaton, E. J., Torres, M. E., Dugan, B., Heeschen, K., Mountjoy, J. J., Ayres, C., Rose, P. S., Pecher, I. A., Barnes, P. M., LeVay, L. J. (2019): Sedimentation Controls on Methane-Hydrate Dynamics Across Glacial/Interglacial Stages: An Example From International Ocean Discovery Program Site U1517, Hikurangi Margin. - *Geochemistry Geophysics Geosystems (G3)*, *20*, 11, pp. 4906—4921.

DOI: http://doi.org/10.1029/2019GC008603

Geochemistry, Geophysics, Geosystems

RESEARCH ARTICLE
10.1029/2019GC008603

Sedimentation Controls on Methane-Hydrate Dynamics Across Glacial/Interglacial Stages: An Example From International Ocean Discovery Program Site U1517, Hikurangi Margin

E. J. Screaton[1], M. E. Torres[2], B. Dugan[3], K. U. Heeschen[4], J. J. Mountjoy[5], C. Ayres[2], P. S. Rose[6], I. A. Pecher[7], P. M. Barnes[6], and L. J. LeVay[8]

[1]Department of Geological Sciences, University of Florida, Gainesville, FL, USA, [2]College of Earth, Ocean, and Atmospheric Sciences, Oregon State University, Corvallis, OR, USA, [3]Department of Geophysics, Colorado School of Mines, Golden, CO, USA, [4]GFZ German Research Centre for Geosciences, Potsdam, Germany, [5]National Institute of Water and Atmospheric Research, Wellington, New Zealand, [6]Department of Physical and Environmental Sciences, Texas A&M University, Corpus Christi, TX, USA, [7]School of Environmental and Marine Sciences, University of Auckland, Auckland, New Zealand, [8]International Ocean Discovery Program, Texas A&M University, College Station, TX, USA

Key Points:
- Pore water chloride concentrations at a Hikurangi Margin site suggest recent methane hydrate formation
- Simulations suggest that sedimentation rates averaging 0.8 mm/year at this site drive gas hydrate dynamics and recent hydrate formation
- Bottom water cooling during glaciation could counteract the impacts on methane hydrate stability of sea level decrease

Supporting Information:
- Supporting Information S1

Correspondence to:
E. J. Screaton,
screaton@ufl.edu

Citation:
Screaton, E. J., Torres, M. E., Dugan, B., Heeschen, K. U., Mountjoy, J. J., Ayres, C., et al (2019). Sedimentation controls on methane-hydrate dynamics across glacial/interglacial stages: An example from International Ocean Discovery Program Site U1517, Hikurangi Margin. *Geochemistry, Geophysics, Geosystems*, *20*, 4906–4921. https://doi.org/10.1029/2019GC008603

Received 1 AUG 2019
Accepted 22 OCT 2019
Published online 8 NOV 2019

Abstract Dissolved chloride concentrations higher than seawater were observed over a broad depth range in pore water profiles from International Ocean Discovery Program Site U1517 on the Hikurangi Margin. This Cl maximum is not associated with an $^{87}Sr/^{86}Sr$ anomaly, indicating that it is not caused by hydration reactions during ash alteration. We use a numerical modeling approach to examine possible causes for recent gas hydrate formation that can result in the observed Cl high. Our approach considers sedimentation, sea level, and bottom water temperature (BWT) changes due to glaciation as drivers for the downward migration of the base of gas hydrate stability and gas hydrate formation. The modeling results reveal that lowering of sea level during glaciation can allow methane hydrate dissociation followed by postglacial hydrate formation as sea level rises. However, BWT cooling of 2 °C during glaciation followed by warming during deglaciation would mostly counteract the impacts of sea level change. Bottom water cooling during glaciation is expected in this region and many locations worldwide. As a result, our simulations do not support the previous hypotheses of large-scale gas hydrate dissociation due to sea level drop during glaciation, which have been proposed as triggers for widespread gas release and slope failure. Such a mechanism is only possible where BWT remains constant or increases during glaciation. Our simulations indicate that sedimentation constitutes the largest factor driving recent methane hydrate formation at Site U1517, and we suggest that sedimentation may play a larger role in gas hydrate dynamics along margins than previously recognized.

Plain Language Summary Methane hydrate, which is a solid material/compound containing methane within frozen cages of water molecules, forms in continental margin sediments beneath the seafloor within a limited range of temperature and pressure. Researchers have previously suggested that sea level change during glaciations would allow methane hydrate to destabilize. This could free methane, cause slope failures, and affect Earth's climate. Drilling of sediments at a site offshore of New Zealand found evidence for recent trapping of methane as hydrate, and we investigate whether the hydrate formation is related to sea level changes associated with glaciation. We use computer models to test how methane hydrate storage would change through 400,000 years of variations in sea level and bottom water temperature. We find that expected water temperature changes during glacial cycles partially counteract the pressure effects of sea level changes. Rapid burial by sediment deposition appears to be the largest factor in storage and release of methane from hydrates at this site and perhaps at other continental margins worldwide.

1. Introduction

Carpenter (1981) first suggested that gas hydrate dissociation during the last glacial maximum (LGM) may have enhanced the frequency of seafloor slumping on continental margins due to release of methane and generation of excess pore pressures. Mapped slope failures in areas of gas hydrate occurrence have been dated to post-LGM in locations such as offshore Norway (8.1 ka), Mauritania (10.5–10.9 ka), the U.S. offshore

of the Carolinas (past 30 ka), and elsewhere (e.g., Henrich et al., 2008; Hornbach et al., 2007; Sultan et al., 2004). The link between slope stability and methane hydrates has been difficult to confirm because other factors besides methane hydrate dissociation may be important in driving slope failure (e.g., Hornbach et al., 2007), and other variables besides sea level change can impact methane hydrate dynamics. In high latitudes, pressure changes associated with isostatic rebound during deglaciation appear to play a key role in gas hydrate dissociation (Wallmann et al., 2018) and glacigenic sediment pulses can have an indirect effect on gas hydrate dynamics (e.g., Karstens et al., 2018). Glacigenic sediment pulses can also directly affect pore pressures and thus slope stability (e.g., Sultan et al., 2004).

Paull et al. (1991) carried further the idea of gas hydrate dissociation driven by climatic perturbations and postulated that significant release of methane at glacial maxima results in warming that limits glaciation. Kennett et al. (2003) also suggested a link between Quaternary intervals of rapid warming and methane hydrate release and termed this the clathrate gun hypothesis. However, Sowers (2006) found no evidence for large contributions from methane hydrate in isotopic analyses of methane in Greenland ice cores. Based on modeling, Mestdagh et al. (2017) concluded that the extent and rate of methane release are too small to have contributed to any significant climate variations at the LGM. Furthermore, consumption of methane by microbial activity in both aerobic and anaerobic conditions within the sediment and the water column acts to prevent much of this greenhouse molecule from reaching the atmosphere (e.g., Ruppel & Kessler, 2017).

In addition to consumption by microbial activity, methane from hydrate dissociation can be recycled to form new hydrate, as postulated by Paull et al. (1994). Li et al. (2017) suggest that methane is recycled offshore Mauritania based on observations of shoaling of the base of gas hydrate stability (BGHS) in seismic reflection profiles and simulations of bottom water temperature (BWT) changes since the LGM. Nole et al. (2018) simulated methane recycling in an area of high sedimentation; as sediment is carried below the BGHS, methane is released during hydrate dissociation, and new hydrate forms higher in the sequence. In contrast, Portilho-Ramos et al. (2018) used foraminifer data from the Brazilian margin to postulate that methane from dissociation was released at the seafloor during the last glacial period (40–20 ka).

The conflicting conclusions in the literature demonstrate the need to better understand the various factors that control gas hydrate stability across glacial/interglacial cycles and their significance in slope stability and methane input into the hydrosphere and atmosphere. Here we evaluate the relative importance of sedimentation, sea level, and BWT changes during glacial/interglacial cycles as potential modulators of gas hydrate stability zones. A numerical modeling approach is applied to conditions at International Ocean Discovery Program Site U1517 on the Hikurangi Margin offshore of the east coast of New Zealand. At this site, a broad high in pore water chloride concentrations is observed between 81 and 179 mbsf. We first use dissolved strontium and its isotopic composition to ascertain that the chloride high is not driven by hydration reactions associated with ash alteration and formation of diagenetic aluminosilicates but is instead the result of other hydration reactions, likely gas hydrate formation. Our model then examines whether the hydrate formation suggested by the observed chloride high could be caused by recent downward migration of the BGHS following the LGM. Results from this modeling provide insights on gas hydrate dissociation and formation in response to sea level and BWT changes and point to the significance of sedimentation as a major factor driving gas hydrate dynamics in this margin.

2. Site U1517 on the Hikurangi Margin

Site U1517 is located in ~725-m water depth within the extensional, creeping part of the Tuaheni Landslide Complex (TLC) east of New Zealand's North Island (Figures 1a and 1b). This area was drilled in two locations (GeoB20803 and GeoB20131) using the MeBo system during the SLAMZ RV Sonne expedition in 2016 (Huhn, 2016). Because the MeBo drilling only reached 80 mbsf at GeoB20131 and recovery was poor between 28 and 60 mbsf, Site U1517 was drilled at this same location during International Ocean Discovery Program Expedition 372 (Pecher et al., 2019). Drilling was designed to test whether methane hydrate, which can form in sediments in water depths greater than 650 m on the Hikurangi Margin (Pecher et al., 2017), contributes to the inferred creeping behavior of this landslide complex (Mountjoy et al., 2014). Based on interpretations of seismic data (Figure 1b), the base of the slide mass occurs at 59 mbsf. A shallower discontinuity at 37 mbsf may represent a possible decollement for creeping (Pecher et al., 2019).

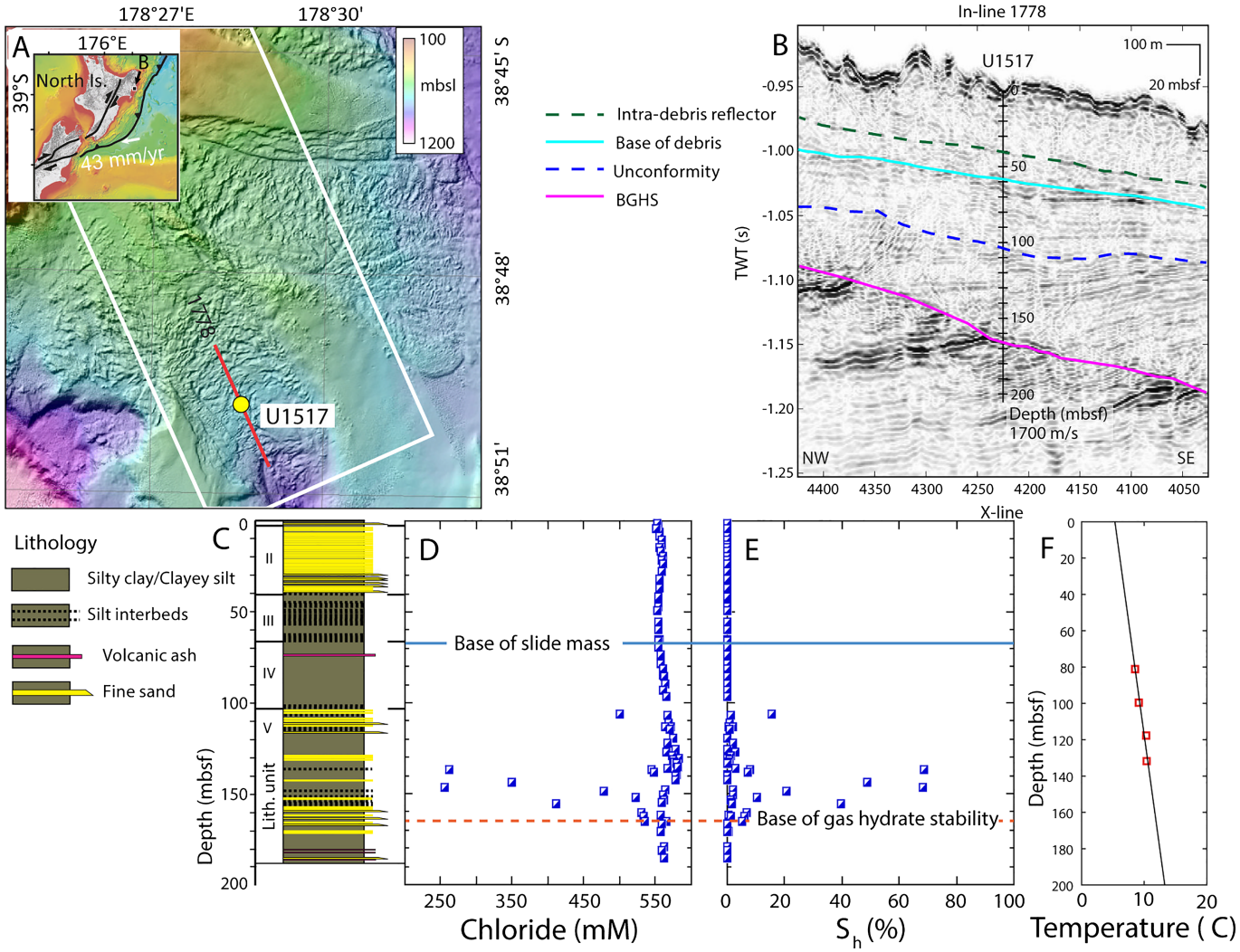

Figure 1. (a) Location map, (b) seismic section with the vertical axis showing two-way traveltime (TWT), (c) Site U1517 lithologic column, (d) sulfate-corrected chloride concentrations, (e) computed gas hydrate saturation, and (f) in situ temperatures. Dashed line shows steady state temperature profile for a bottom water temperature of 6.5 °C and a thermal gradient of 0.27 °C/m.

Drilling at Site U1517 recovered hemipelagic sediments, bedded turbidite sequences, and mass transport deposits (MTDs) to a depth of 188.5 mbsf (Figure 1c; Pecher et al., 2019). Recovered sediments in the upper 3 mbsf are Holocene in age, and underlying sediments are Pleistocene, ranging in age up to 50 ka. The biostratigraphy indicates an average sedimentation rate of 0.8 mm/year (Pecher et al., 2019). Because this is a dynamic region, sedimentation rates are likely to be variable, and much of the sedimentary sequence could be deposited during punctuated events. Lithologic observations assign the interval from 3.3 to 66.6 mbsf to the TLC debris unit (Pecher et al., 2019), an inference that is consistent with high-resolution (chirp) seismic as well as 2-D and 3-D multichannel seismic data interpretations that place the base of TLC landslide debris at 59 mbsf (Gross et al., 2018; Kuhlmann et al., 2018; Mountjoy et al., 2014). Four in situ temperature measurements provide information on thermal conditions. Shipboard analysis suggested a temperature (T; °C) and depth (mbsf) relationship of $T = 5.32 + 0.0398 \times$ depth (mbsf; Pecher et al., 2019).

In addition to routine samples for pore water chemistry, additional pore water sampling of Site U1517 cores was guided by cold temperature anomalies in infrared scans. These anomalies were interpreted to indicate the occurrence of gas hydrate dissociating following recovery of the sample. Dissolved chloride concentrations, measured by both titration and by ion chromatography (Pecher et al., 2019), reveal a broad high between 81 and 179 mbsf, with values as high as 582 mM (Figure 1d). Based on salinities recorded on the Hikurangi Margin (Faure et al., 2010), bottom water here has a chloride concentration of ~540 mM.

Superimposed on this overall trend are discrete excursions to lower chloride values in the gas hydrate stability zone, similar to those previously observed in pore waters recovered from gas hydrate-bearing sediments (Riedel et al., 2006; Torres et al., 2008; Tréhu et al., 2004).

Estimates of gas hydrate abundance are commonly based on the magnitude of discrete excursions to anomalously low chloride values, which represent freshwater release from gas hydrate that dissociated during core retrieval (e.g., Ussler & Paull, 2001). An empirical approach was used to estimate a gas hydrate saturation value S_h based on the concentrations in the discrete chloride anomalies and the estimated background chloride concentration (Malinverno et al., 2008):

$$S_h = [a\ (C_b - C)]/[C + a\ (C_b - C)], \quad (1)$$

where C is the sulfate-corrected chloride concentration measured in the discrete chloride anomalies after gas hydrate dissociation in the core samples; C_b is the estimated background chloride concentration, which is defined as the envelope of measurements around the discrete chloride anomalies (e.g., Torres et al., 2008); and a is a dimensionless constant that quantifies the density change due to gas hydrate dissociation and equals 1.257 (Malinverno et al., 2008).

The Site U1517 chloride data indicate the presence of discrete gas hydrate occurrences between ~100 and 165 mbsf, typically within thin intervals of coarser sediment (Figure 1e). Occurrence of gas hydrates in thin coarse layers is commonly observed and has been attributed to diffusion of methane into sediments with larger pore sizes where hydrate growth is favored (e.g., Malinverno, 2010). S_h values range from 2% to 68%, and no evidence for gas hydrate was found above 100 mbsf. Because the pore water measurements targeted intervals of potential hydrates, these results are biased to larger S_h values. Logging-while-drilling measurements of resistivity and porosity provide a less-biased estimate of S_h values, determining average values over a depth interval of a few tens of centimeters (Pecher et al., 2019). These estimates yield S_h generally varying between 0% and 10%, with some intervals (113.0–113.3, 117.5–121.0, and 128.0–145.5 mbsf) exceeding 20% (Pecher et al., 2019).

3. Factors Affecting Chloride Profiles

In this investigation, we explore the possibility that the dissolved chloride profile at Site U1517 reflects the uptake and release of water as gas hydrate forms and dissociates. Gas hydrate formation/dissociation changes dissolved chloride concentrations, which may be used to infer the timing and forcings involved in gas hydrate dynamics. Significant increases in dissolved chloride concentrations associated with shallow massive gas hydrate deposits in Hydrate Ridge offshore Oregon (Haeckel et al., 2004; Torres et al., 2004) and elsewhere (Torres et al., 2011) were used to document rapid gas hydrate formation near the seafloor sustained by transport of methane in the gas phase. Bangs et al. (2005) combined analyses of bottom-simulating reflectors in seismic data from Hydrate Ridge with a broad freshening signal in pore fluids at ODP Site 1247 to postulate an episode of gas hydrate destabilization that occurred ~4 to 8 ka, following postglacial warming. Similarly, a broad freshening signal in pore fluids recovered by MeBo drilling off Svalbard was attributed to an enhancement in gas hydrate dissociation driven by isostatic rebound (Wallmann et al., 2018).

The studies discussed above relied on the fact that chloride is highly conservative during early diagenesis, so that changes in its concentration are driven solely by consumption or release of freshwater. Before investigating gas hydrate dynamics, it is important to consider additional factors that can affect chloride concentrations. Other hydration/dehydration reactions are summarized in Kastner et al. (2014) and include pore fluid freshening during conversion of opal-A to opal-CT/quartz and of smectite to illite. Both these reactions occur at temperatures >60 °C and thus do not commonly occur within the gas hydrate stability zone. Fluid migration and ion diffusion can result in pore fluids with chloride concentrations much lower than seawater values at depths where gas hydrates are present, as observed, for example, offshore Japan, Cascadia, and in the central Ulleung basin (Kim et al., 2013; Torres et al., 2004; Wei et al., 2008). We do not observe these effects at Site U1517.

Chloride enrichment is indicative of reactions that uptake water, which, in addition to gas hydrate formation, can reflect weathering of reactive silicates, such as observed in the Indian margin (Solomon et al., 2014). These alteration reactions can occur at low temperatures, so they can be concomitant with gas hydrate

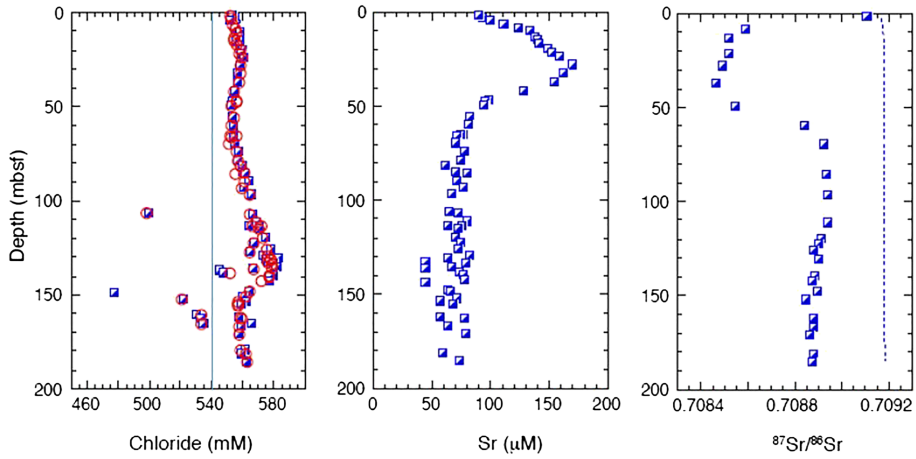

Figure 2. Chloride (blue squares from titration and red circles from ion chromatography), strontium, and $^{87}Sr/^{86}Sr$ profiles of Site U1517. The vertical blue line on the chloride plot shows concentration of 540 mM. The dashed vertical line shows the present-day $^{87}Sr/^{86}Sr$ seawater value.

stability zones. To evaluate whether the observed chloride maxima is the result of recent formation of authigenic aluminosilicates driven by ash alteration, we compare the dissolved chloride data with the strontium concentration and isotopic composition because silicate weathering releases strontium to the pore fluids (Figure 2). In addition, $^{87}Sr/^{86}Sr$ is not affected by biologically induced fractionations and nonbiogenic silicate sources have an isotopic value that is clearly distinct from that of its coeval seawater (e.g., Teichert et al., 2005; Torres et al., 2015). The entire sediment column sampled at Site U1517 is younger than 540 ka. During the time interval from 540 ka to the present, the seawater $^{87}Sr/^{86}Sr$ is similar to the present-day value of 0.70917 (Paytan et al., 1993).

Sr results are shown in Table S1 and were generated following the methods of McCarthy et al. (2018), whichare summarized in Text S1. At Site U1517, there is a marked increase in dissolved strontium in the upper 65 mbsf, concomitant with a significant decrease in $^{87}Sr/^{86}Sr$ values (to 0.708463). These data reflect rapid alteration of volcanic ash, an observation typical of active margins worldwide (e.g., Nankai, Sample et al., 2017; Costa Rica, Ross et al., 2015; Antilles, Murray et al., 2018). The isotopic composition of fluids below 60 mbsf is lower than expected coeval seawater values but are relatively uniform, likely reflecting an early ash alteration signal that has been smoothed by diffusion. There is no $^{87}Sr/^{86}Sr$ anomaly that corresponds to the broad chloride maximum between 81 and 179 mbsf, indicating that the chloride anomaly observed in this interval is not associated with recent ash alteration reactions. We argue that this chloride signal reflects gas hydrate formation.

4. Numerical Modeling Methods

We use a numerical modeling approach that incorporates sea level and BWT changes, sedimentation, solute and thermal diffusion, and latent heat effects. Thermal and chloride diffusion are simulated using a one-dimensional fully implicit finite difference model. The sediment column is discretized with a 0.8-m vertical spacing, and a simulation time step of 1,000 years is used. This time step and vertical spacing are consistent with the average sedimentation rate so that steady sedimentation can be simulated by adding one cell each time step. Downward advection of heat, pore water chloride concentrations, and hydrate are simulated by shifting these values downward when sedimentation occurs. In addition to steady sedimentation, simulations will also examine the impacts of variable sedimentation pulses, including rapid emplacement of MTDs.

Because this investigation focuses on the overall magnitude and depth range of the elevated chloride rather than small-scale variations, the modeling approach is simplified by applying uniform, average values for porosity, thermal properties, and diffusion coefficients. Pore water data at Site U1517 show no indication of fluid migration, and the porosity profile at Site U1517 does not show a compaction

trend (Pecher et al., 2019). Thus, advection of heat and chloride due to fluid flow are not simulated. Although fluid advection due to compaction is not simulated for Site U1517, chloride transport by advection could be significant at other locations with similar sedimentation rates; the upward fluid advection would reduce the impact of downward movement due to sedimentation (Text S2). The upward fluid flow velocity would depend on total thickness of sediment, compaction properties of the sediment, sediment permeability values, and whether all expelled water moves vertically or some escapes through faults or laterally.

The governing equation for one-dimensional diffusive solute flux incorporates Fick's law into a mass balance equation:

$$D\frac{\partial^2 C}{\partial z^2} + R_S = \frac{\partial C}{\partial t}, \tag{2}$$

where D is the diffusion coefficient for a porous media, C is concentration, z is depth, R_s is a solute source/sink term that includes net gains or losses due to reactions, and t is time. For the simulations, we compute D from the diffusion in seawater, D_{sw}, and porosity, n, by (Boudreau, 1996)

$$D = \frac{D_{sw}}{[1-\ln(n^2)]}. \tag{3}$$

For Site U1517, porosity of 0.46 is assigned based on an average of the shipboard measurements (Pecher et al., 2019), and D_{sw} for chloride in seawater is assumed to be 1.3×10^{-9} m^2/s.

The governing equation for one-dimensional transient conductive heat flow, expressed in terms of temperature, T (°C), combines Fourier's law of heat conduction with conservation of energy:

$$\frac{\kappa}{c\rho_f}\frac{\partial^2 T}{\partial z^2} + R_h = \frac{\partial T}{\partial t}, \tag{4}$$

where κ is the thermal conductivity of the medium, R_h is a heat source/sink term, ρ_f is the fluid density, and c is the heat capacity of the medium. In these simulations, we apply an uniform κ of 1.6 W/(m·°C), based on a weighted average of solid and water thermal conductivities of 0.7 and 3.0 W/(m·°C), respectively. This is higher than the average shipboard measurement of 1.2 W/(m·°C). Because shipboard measurements are conducted at room temperature and pressure, they likely underestimate in situ values. Bulk density of 1,900 kg/m^3 and heat capacity of 2,400 J/kg·°C are also based on weighted averages for a porosity of 0.46.

In situ temperature measurements from Site U1517 (Figure 1f) provide information on heat flow but have some uncertainty because the data only cover a small depth range and BWT was not measured during the expedition. Previous water column measurements in the Tuaheni area suggest that temperatures at 725 mbsf are >7 °C (Mountjoy et al., 2014), which is significantly higher than the 5.32 °C inferred from the Site U1517 extrapolation. For most simulations, a BWT value of 6.5 °C and a basal heat flow of 0.043 to 0.050 W/m^2 are used. The heat flow is enforced by a boundary condition at the base of the simulated sediment column. Similar results (Figure S1) are obtained using a BWT of 5.32 °C and a heat flow of 0.064 W/m^2, consistent with the thermal gradient of 39.8 °C/km reported by Pecher et al. (2019).

Stability of methane hydrate is estimated using the predictive relationship of Dickens and Quinby-Hunt (1994):

$$1/(273.15 + T) = 3.79{*}10^{-3} - 2.83{\times}10^{-4}(\log P), \tag{5}$$

where P is pressure (Pa). The Dickens and Quinby-Hunt (1994) relationship is based on experiments using seawater and pressures up to 10 MPa, which is sufficient for Site U1517 conditions. In this pressure range (<10 MPa), comparison of the Dickens and Quinby-Hunt (1994) and Sloan (1998) relationships indicate that they yield similar results (O'Regan & Moran, 2010).

Dissociation and formation of methane hydrate consume and release energy, respectively. The effects of latent heat are incorporated into the modeling as follows. During each simulation time step, cells in the

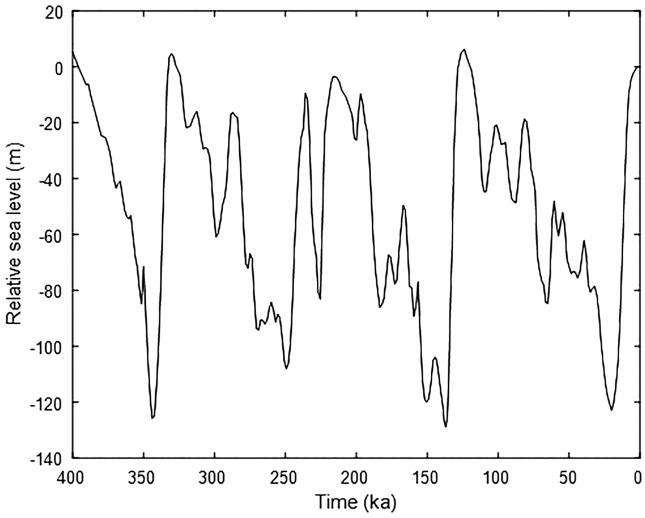

Figure 3. Relative sea level based on the results of Waelbroeck et al. (2002).

column are checked as to whether hydrate is stable or unstable according to equation (5). If hydrate is unstable and the hydrate saturation is greater than 0, dissociation is allowed. On the other hand, hydrate formation is allowed if hydrate is stable, and the hydrate saturation is less than an allowed maximum. The maximum allowed S_h for most simulations was 4% to 5%, although greater and lesser values were tested. This value was based on the observations concerning hydrate saturation at Site U1517, with analyses of resistivity-while-drilling results yielding values ranging between 0% and 10% and thin intervals of 20% (Pecher et al., 2019). Sensitivity testing simulations (Figure S2) suggest that S_h values greater than 6% would result in a pore water chloride anomaly higher than observed.

To determine the volume of hydrate that can form or dissociate, the available energy is computed using the bulk density and heat capacity of the porous media multiplied by the difference between the temperature in the cell and the stability temperature at that depth (equation (5)). Temperature within the cell is reduced or increased based on the energy consumed or released. Methane hydrate saturation is not allowed to fall below 0 or to increase to greater than a prescribed maximum.

Latent heat of methane hydrate formation/dissociation of 430 kJ/kg was assumed for the simulations (e.g., Nole et al., 2018). Changes in chloride concentration due to hydrate formation or dissociation are calculated based on the relationship shown in equation (1).

For most simulations, we set an upper depth threshold for methane hydrate formation at 100 mbsf, based on the observations from Site U1517 (Pecher et al., 2019). For methane hydrate to form, methane concentration must be higher than the amount required to thermodynamically form gas hydrate at a given temperature/pressure conditions (Claypool & Kaplan, 1974). Methane concentrations are controlled by accumulation of particulate organic carbon at the seafloor, the rate of methane generation in marine sediments, and the ascent of deep-seated pore fluids and methane gas (e.g., Malinverno et al., 2018; Wallmann et al., 2012); the top of methane hydrate can commonly be expected to occur at 10 to 12 times the depth of the sulfate-methane transition (Bhatnagar et al., 2011). At Site U1517, the sulfate-methane transition was observed at 15 to 17 mbsf and methane concentrations quickly increased below this depth (Pecher et al., 2019). We assume that there is enough methane to support gas hydrate formation below 100 mbsf to reach the 4% to 5%, as described above. We note that this methane supply could include methane recycled from previous dissociation of methane hydrate or can be supplied from deeper sources where seismic data indicate the presence of methane gas. It is also possible that more or less methane hydrate was able to form in the past due to variations in methane supply and loss.

Selecting initial conditions for the simulation is challenging because no information exists about past hydrate saturation, chloride concentration, or thermal conditions at depth. As computed by Ussler and Paull (2001), a 10-m (5-m half space) thick anomaly can dissipate to <12.5% of its initial value in 40,000 years due to diffusion. However, a thicker anomaly would take much longer to dissipate (>100,000 years), and the choice of initial conditions could impact the final chloride profile if only one glacial cycle were simulated. To reduce the impact of the initial conditions, the simulation is begun at 400 ka, although only the results from 120 ka to the present are presented. The 400-ka sediment column is assigned a chloride concentration averaging glacial and interglacial values, a steady state thermal profile based on the specified heat flow, and methane hydrate at the maximum allowed S_h at depths between the applied top of hydrate and 165 mbsf.

Water depth through time at the site is computed using a present seafloor depth of 725 m and global sea level changes from Waelbroeck et al. (2002) (Figure 3). For calculation of hydrate stability, fluid pressure throughout the sediment profile is changed instantaneously with sea level due to the changing height of the overlying water column. Bottom water chloride concentration and temperature are simulated to vary with sea level change. It is assumed that chloride concentration is 3% higher when sea level is 120 m lower (Adkins et al., 2002). A present-day value of 548 mM was used for the simulations. This value is based on a visual fit between the simulated chloride profile and the Site U1517 results in the upper 40 m.

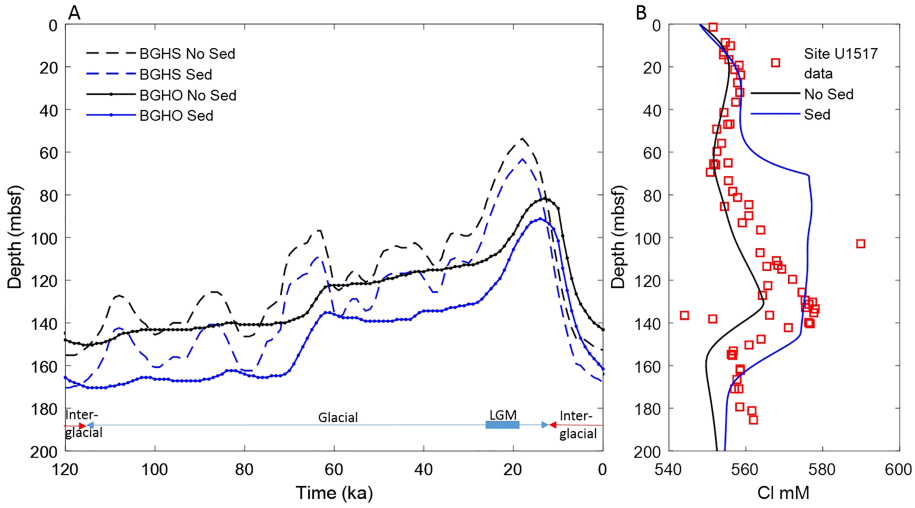

Figure 4. Simulated changes in hydrate stability and occurrence at Site U1517 due to glacial-interglacial sea level changes and constant bottom water temperature. Simulations with no sedimentation are shown in black and with 0.8-mm/year sedimentation are shown in blue. (a) Depths of the BGHS (dashed) and the BGHO (solid line with dots). (b) Observed Site U1517 chloride concentrations (red) and simulated chloride profiles without sedimentation (black) and with 0.8-mm/year sedimentation (blue). BGHO = base of gas hydrate occurrence; BGHS = base of gas hydrate stability; LGM = last glacial maximum.

BWT at this location during the LGM is not known. Oxygen isotope results from core MD97-2121 (Carter et al., 2008; 2,314-m water depth, 180 km to the SE of Site U1517) suggest cooling of ~2 °C at the LGM, and we test the impacts of this magnitude of cooling with the simulations. Temperature and chloride concentration were assigned to remain constant through time at the bottom boundary, and the base of the model (800 mbsf) is set significantly below the depth of interest (<200 mbsf) to minimize the effect of the bottom boundary conditions.

5. Results and Discussion

As a first step, we simulate the impact of sea level change on gas hydrate stability and chloride concentrations, both without and with sedimentation (Figure 4). The simulations in Figure 4 use a BWT of 6.5 °C, heat flow of 0.043 W/m^2, and a maximum hydrate saturation of 5%. For this initial step, we set the minimum depth to 60 mbsf, slightly shallower than hydrate observed at Site U1517, to better illustrate the range of variations in the base of gas hydrate.

In the results, we will use the term BGHS to indicate the depth calculated from equation (5) prior to calculation of hydrate formation/dissociation and related heating/cooling (e.g., latent heat effects). We then calculate hydrate formation/dissociation and denote the depth below which $S_h < 1\%$, as the simulated base of gas hydrate occurrence (BGHO). In the simulation without sedimentation, the BGHS shallows as sea level drops during glaciation (120 to 20 ka) and deepens during deglaciation (Figure 4a), in agreement with predictions by Paull et al. (1991). The simulated BGHO responds more slowly than the BGHS due to latent heat effects (Figure 4a). As a result, gas hydrate remains beneath the BGHS as the BGHS moves upward during glaciation (Figure 4a). The greatest difference in depth (35 m) between the BHGS and BGHO occurs 22 ka, following an interval of rapid sea level decline and rapid shoaling of the BGHS. During deglaciation and sea level rise, the BHGS moves downward more rapidly than hydrate can form. As a result, the simulated BGHO is shallower than the calculated BGHS from 13 ka to the present.

The recent (post-LGM) methane hydrate formation produces a chloride maximum roughly consistent in shape to that observed at Site U1517, although smaller in magnitude (Figure 4b). Dissociation and formation of hydrate occur within the same sediments, and the chloride concentration would return to its initial value if there were no diffusion. With diffusion, the decrease in chloride concentration caused by dissociation during glaciation and sea level decline is dissipated over tens of thousands of years. In contrast, recent (<13 ka)

formation of methane hydrate and the resulting increase in chloride concentration has had much less time to be smoothed by diffusion.

We next consider the effects of constant sedimentation by applying the average Site U1517 sedimentation rate of 0.8 mm/year (Figure 4). We assume that additional sediment thickness is offset by underlying compaction or subsidence, resulting in no change in seafloor depth. At the start of each 1,000-year time step, the uppermost cell is assigned the chloride concentration and temperature of bottom water and has no methane hydrate. Underlying cells are shifted downward, carrying their chloride concentration, temperature, and hydrate saturation values.

With 0.8-mm/year sedimentation, the simulated BGHS is deeper than for the case with no sedimentation due to the cooling effect of rapid burial of seafloor sediment and its pore water (Figure 4a). For example, the simulation with sedimentation has a temperature 0.17 °C cooler at 150 mbsf than the simulation without sedimentation. As a result of cooler temperatures with sedimentation, the simulated BGHS averages 14 m lower. Although the simulated BGHS is deeper in the simulation with 0.8-mm/year sedimentation, the sedimentation is still pushing hydrate-bearing sediment downward and resulting in dissociation of hydrate beneath the BGHS. There is a larger offset between the BGHS and the BGHO in the simulation with 0.8-mm/year sedimentation than without sedimentation because sedimentation buries hydrate below the BGHS more rapidly than it can dissociate. In this respect, the simulations help to demonstrate the potential difficulty in comparing field observations of gas hydrate occurrence with theoretical calculations of gas hydrate stability.

As sediment is deposited and buried, methane hydrate forms and chloride concentrations increase. In Figure 4a, the enforced shallowest depth of hydrate formation is at 60 mbsf. This artificial boundary causes simulated chloride concentration to increase sharply near this depth (Figure 4b). In reality, the actual increase would be more gradual than simulated due to methane availability. Sediment pore size would also affect the depth of hydrate formation and alter the shape of the chloride profile because methane hydrate preferentially forms in larger pores (e.g., Daigle & Dugan, 2014).

As continuous burial pushes sediment to beneath the BGHS, dissociation can occur and chloride concentrations decrease (Figure 4b). The lower boundary of the chloride high is ~20 m deeper in the simulation with sedimentation than without, likely due to the cooling effect of sediment burial and the fact that sedimentation carries gas hydrate downward through the sediment column.

Additional simulations assess how BWT variations during glacial cycles would impact gas hydrate formation/dissociation and the chloride profile. For these simulations, applied BWT changes are estimated to vary linearly with sea level, with a BWT of 4.5 °C assigned when sea level is 120 m lower than the present and a BWT of 6.5 °C assigned when the sea level is the same as at the present. This represents overall cooling during glaciation and warming during deglaciation but does not include local effects on BWT due to changes in currents. Due to the cooler temperatures entering the sediments from the seafloor during the past, the basal heat flow is increased to 0.050 W/m^2 so that temperatures at the depths of interest remain approximately the same as the constant BWT simulation and consistent with the present-day observed temperatures.

Results of this exercise demonstrate that the behavior of methane hydrate is very different with a 2.0 °C BWT cooling during the LGM than with constant BWT (Figure 5a). Both the BGHS and the BGHO show much less variability than for the simulations with constant BWT because cooling during glaciation and warming during deglaciation counteract the impact of sea level fall and rise. As a result, the depth of hydrate occurrence is relatively constant for much of the simulated time. There are some variations during very rapid changes in sea level such as 120 to 100 ka and from ~12 ka to the present (Figure 5a), due to the time lag for the BWT change to diffuse into the sediments. In the case with no sedimentation (Figure 5b), the resulting chloride profile has a much smaller chloride maximum than with constant BWT (Figure 4b). In contrast, the chloride profile with sedimentation retains a significant high-chloride anomaly. This observation hints at the significant effect that sedimentation can have on changes in gas hydrate dynamics.

For the simulations shown in Figures 5, the minimum depth of hydrate formation was assigned to be 60 mbsf and the maximum hydrate saturation is 5%. The visual match to the Site U1517 chloride data can be improved by increasing the minimum depth to 100 mbsf, consistent with the observations at Site U1517, and reducing the maximum hydrate saturation to 4% (Figure 6). These values are used consistently for

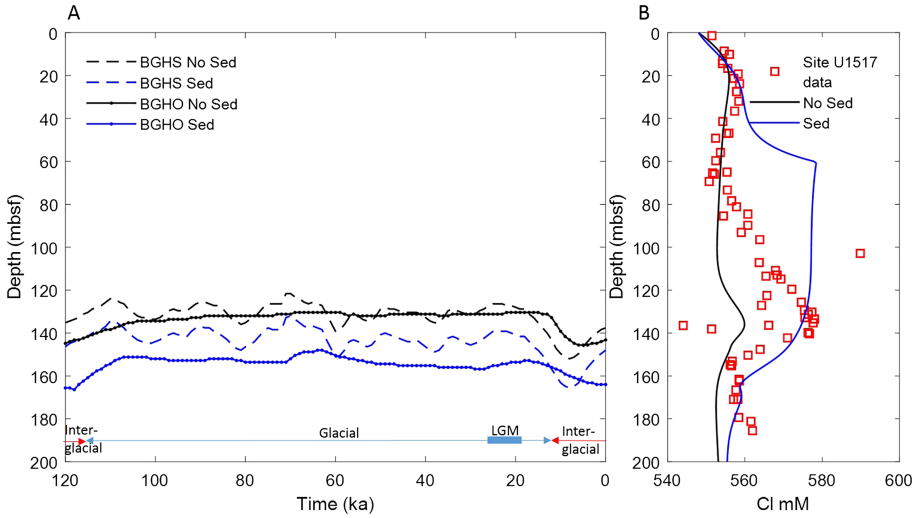

Figure 5. Simulated changes for a 2 °C decrease in bottom water temperature with no sedimentation (black) and with 0.8-mm/year sedimentation (blue). (a) Depths of the BGHS (dashed) and the BGHO (solid line with dots). (b) Observed Site U1517 chloride concentrations and simulated chloride profiles with no sedimentation (black) and with 0.8-mm/year sedimentation (blue). BGHO = base of gas hydrate occurrence; BGHS = base of gas hydrate stability; LGM = last glacial maximum.

subsequent simulations. In addition to the results discussed below, we test sensitivity to BWT and heat flow (Figure S1) and maximum hydrate saturations of 2%, 4%, and 6% (Figure S2). Simulated thermal profiles for all simulations are presented in Figure S3.

To further understand the role of sedimentation, we conduct a simulation with constant sea level and BWT constant, so that the only perturbation is due to sedimentation (Figures 6a and 6b). With no sea level or BWT changes, the BGHS remains constant through time (Figure 6a). The sediment moves downward, displacing hydrate to beneath the BGHS where it will dissociate. Throughout the simulation, the BGHO remains 10.4 m below the BGHS. Due to latent heat effects there is a time lag after the sediment passes below the BGHS before the gas hydrate saturation decreases below 1%; burial by an additional 10.4 m below the BGHS allows 13,000 years for the methane hydrate to dissociate.

The chloride profile is similar with and without sea level and BWT changes, demonstrating that the impacts of sedimentation, rather than oceanographic changes associated with glacial/interglacial cycles, dominate the simulated chloride profile at Site U1517. When sedimentation is the only forcing considered, chloride concentrations between ~130 and 180 mbsf are slightly lower than when oceanographic changes are also included.

The impact of sedimentation appears dominant when the sedimentation rate is 0.8 mm/year, so it is useful to assess what occurs at lower sedimentation rates. In Figures 6c and 6d, we compare simulations with 0.4, 0.2, and 0.1-mm/year sedimentation rates to the Site U1517 average of 0.8 mm/year. The simulation with 0.1 mm/year yields results similar to the simulation with no sedimentation (Figure 6b). In contrast the 0.2- and 0.4-mm/year sedimentation rates result in notable chloride anomalies, although the shape differs from the 0.8-mm/year simulation (Figure 6b). The simulations shown in Figures 5 and 6 illustrate that steady sedimentation can significantly impact hydrate dynamics when the rate exceeds 0.1 mm/year.

We next test the impact of time-varying sedimentation rates and show the results in Figure 7. Sedimentation rates can vary through time for a variety of reasons. Carter and Manighetti (2006) found that sedimentation rates at core MD97-2121 (180 km to the SE of U1517) are generally higher at the LGM than during interglacial intervals, although the relationship is complicated by the interactions of terrigenous and biogenic sediment supply, sea level, and circulation patterns.

We test sensitivity to variability by using two simulations that both produce an average rate of 0.8 mm/year. In the first, termed “Varying Sed 1,” we apply a sedimentation rate of 1.6 mm/year when sea level is more than 50 m lower than current values and 0 mm/year when sea level is above that threshold. In the second,

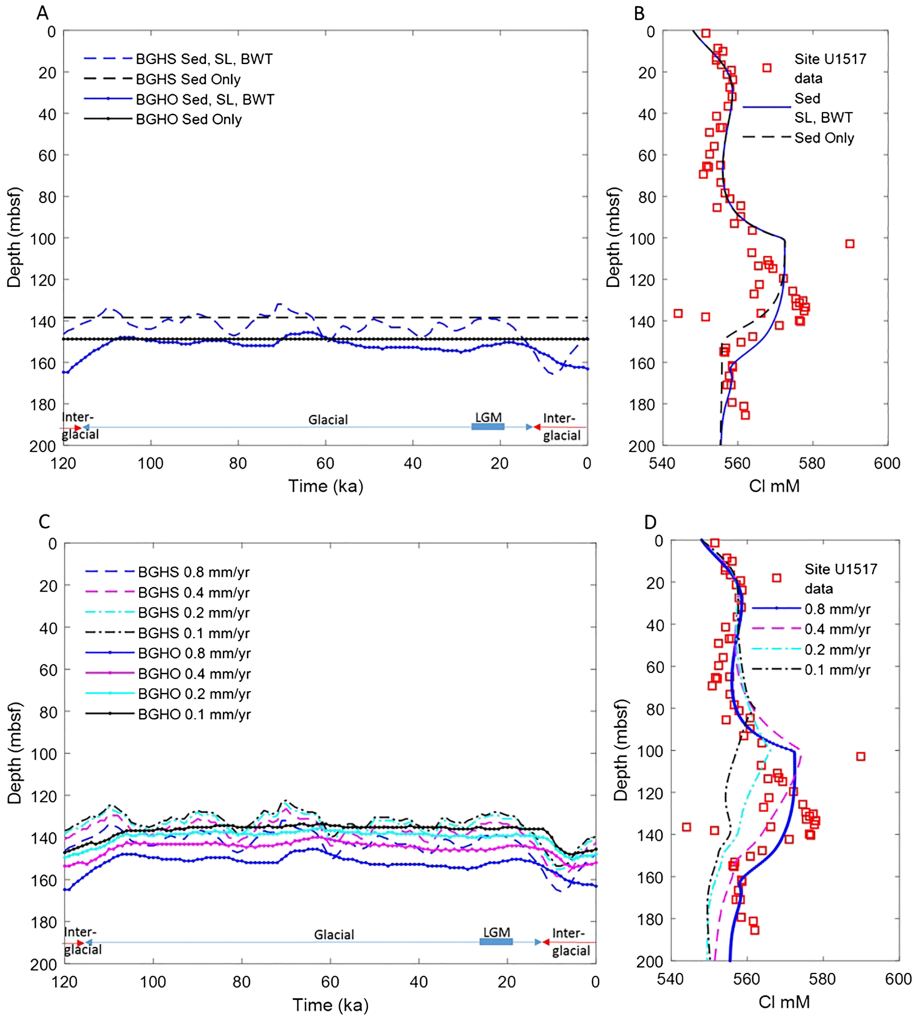

Figure 6. Simulation results for a 2 °C decrease in temperature with constant 0.8-mm/year sedimentation with sea level and BWT changes (blue) and without sea level and BWT changes (black). (a) Depths of the BGHS (dashed) and the BGHO (solid line with dots). (b) Observed Site U1517 chloride concentrations (red squares) and simulated chloride concentrations. (c) Depths of the BGHS (dashed) and the BGHO (solid line with dots) and (d) Observed Site U1517 chloride concentrations (red squares) and simulated chloride profiles with constant 0.8 (blue), 0.4 (magenta), 0.2 (cyan), and 0.1 (black)-mm/year sedimentation rates. BGHO = base of gas hydrate occurrence; BGHS = base of gas hydrate stability; BWT = bottom water temperature; LGM = last glacial maximum.

termed "Varying Sed 2," we apply a sedimentation rate of 0 mm/year during low stands (sea level more than 50 m lower than current values) and 1.6 mm/year when sea level is above that threshold. Although neither simulation is realistic, they serve to illustrate the effects of time-varying sedimentation rate.

Results show that the BGHO is very sensitive to variable sedimentation (Figure 7a), shallowing during the periods of no sedimentation (~120 to 72 ka and ~12 to 0 ka for the Varying Sed 1 simulation and ~72 to 12 ka for the Varying Sed 2 simulation) and deepening when sedimentation rates are high. Despite the difference in the BGHO through time, the Varying Sed 1 chloride profile is similar to the case with constant sedimentation. There is a broad zone of high chloride concentrations, likely due to recent methane hydrate formation between 72 and 12 ka. In contrast, the Varying Sed 2 simulation results in a much narrower chloride high centered between 100 and 120 mbsf. Although hydrate has recently (12 ka to the present) formed, the dissociation of hydrate between 72 and 12 ka caused low chloride concentrations that has not yet diffused.

Finally, we test two scenarios with sudden deposition due to the emplacement of a MTD (Figures 7c and 7d). For both, we assume that MTD emplacement occurs at the start of the Holocene, based on the age of the 0- to 3-m sediments at Site U1517. In the "Slide 1" simulation, the full 60 m is deposited in one time step at 11 ka.

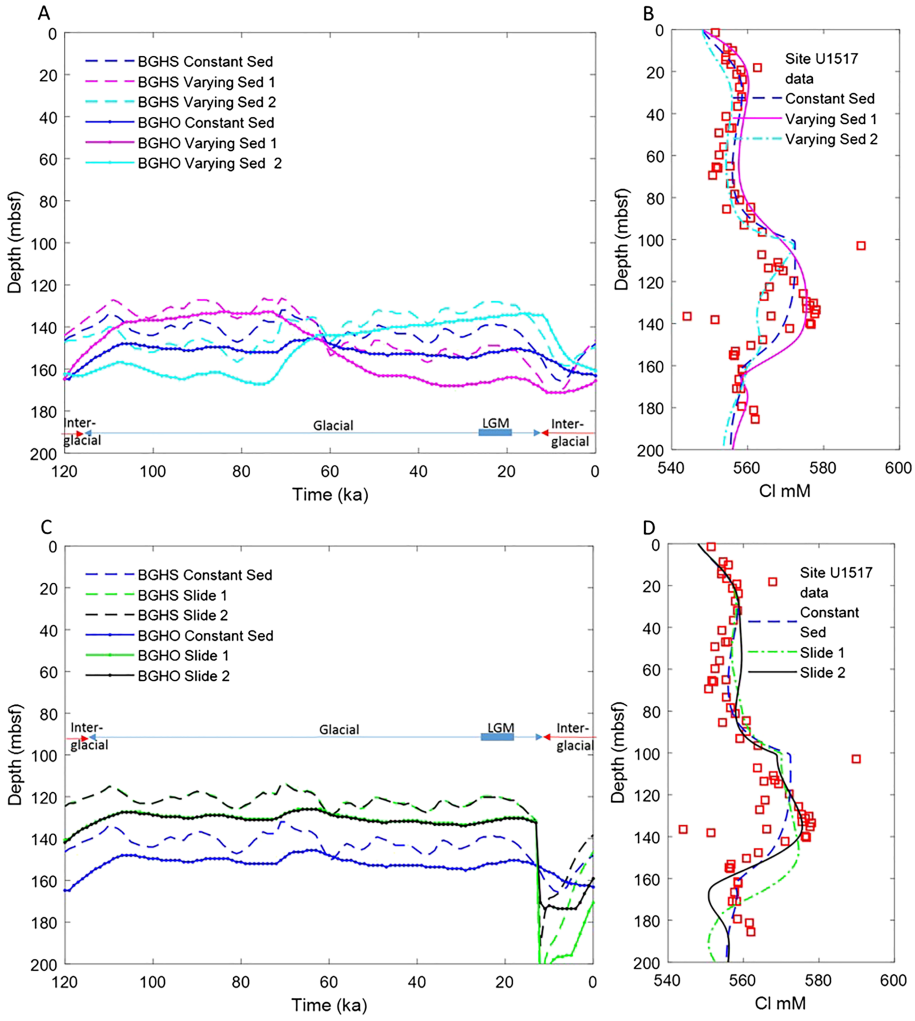

Figure 7. (a) Depths of the BGHS (dashed) and the BGHO (solid line with dots) and (b) chloride profiles with constant 0.8-mm/year sedimentation (blue), sedimentation only during low stands occurring ~72 to 12 ka ("Varying Sed 1," magenta), and sedimentation only during high stands or ~120 to 72 ka and ~12 to 0 ka ("Varying Sed 2," cyan). (c) Depths of the BGHS (dashed) and the BGHO (solid line with circles) and (d) chloride profiles with constant 0.8-mm/year sedimentation (blue), a 60-m slide ("Slide 1," green), and a 37-m slide ("Slide 2," black). BGHO = base of gas hydrate occurrence; BGHS = base of gas hydrate stability; LGM = last glacial maximum.

In the "Slide 2" simulation, the 37 m above the possible decollement is deposited at 11 ka. The MTD is assumed to have been deposited as a block, so the simulation repeats the temperature and chloride concentration of the upper part of the profile rather than assigns the properties of bottom water. Prior to the MTD emplacement, uniform deposition is simulated with rates (0.68 mm/year for "Slide 1" and 0.72 mm/year for "Slide 2) that result in the same overall average sedimentation rate of 0.8 mm/year. Because the MTD emplacement rapidly buries seafloor and shallow sediments, the sediment directly underneath the MTD initially is anomalously cool. This cooling effect of the rapid emplacement of the MTD requires increasing the heat flow to 0.055 W/m^2 to yield simulated temperatures consistent with Site U1517 data.

The BGHS and BGHO drop at 11 ka in both slide simulations. The simulated MTD emplacement displaces hydrate downward and also perturbs the thermal profile by rapidly burying cooler sediment. After the slide, the BGHS rises as temperatures begin to equilibrate. The BGHO shallows more slowly and does not have time to reach its pre-slide depth. Both slide simulations yield chloride profiles with broad, rounded highs, with the 37-m thick MTD producing a profile more similar to the observations (Figure 7d). The MTD buries the high-chloride signature of hydrate that formed prior to the landslide. As hydrate dissociates during thermal equilibration, the chloride concentration gradually decreases.

6. Implications

Elevated chloride concentrations provide evidence for recent methane hydrate formation beneath the TLC at Site U1517. The simulations presented here suggest that although methane hydrate formation can occur in response to sea level change driven by glacial cycles, a decrease in BWT during glaciation can potentially negate this effect. If 2.0 °C BWT cooling occurred during the LGM, as suggested by investigations offshore the east coast of New Zealand (Carter et al., 2008), the resulting temperature change in the sediments could counteract much of the effect of sea level change on the stability of gas hydrates along the Hikurangi margin.

Based on the simulations of Site U1517, sedimentation averaging 0.8 mm/year, rather than glacially driven sea level changes, appears to be the dominant factor in recent methane hydrate formation and creation of the observed high-chloride anomaly. At shallow depths, hydrate forms as sediment is buried to a depth where sufficient methane is available and dissociates after it is buried beyond its stability limit. The resulting high-chloride anomaly appears broader than that observed at Site U1517, where the profile has likely been modified by factors such as grain size distribution because hydrates tend to form in coarse-grained horizons.

Time-varying sedimentation rates will also alter the shape of the chloride profile. A potential scenario to explain the observed chloride anomaly in the context to the depositional history of the U1517 site is shown (in an exaggerated simulation) by the magenta curves in Figures 7a and 7b. Lowering of sea level during glaciation enhances off-shelf sedimentation, with an associated increase in sedimentation rates on the continental slope and in deep sea basins, as shown in several locations worldwide (e.g., Peizhen et al., 2001). This increase in sedimentation rates deepens the BGHO at the LGM, due to both the cooling effect of high sedimentation and the downward transport of sediments more rapidly than methane hydrates can dissociate. Following deglaciation, continental slope sedimentation rates decrease, and sediment depocenters develop on the continental shelf. As a result, the BGHS experiences a rapid rebound and the BGHO moves upward more gradually. Sea level and BWT changes associated with the glacial/interglacial transition have a much more limited effect, as shown by the small chloride high in our simulation with no sedimentation (black line in Figure 5). Recent, rapid burial due to emplacement of landslide material (Figures 7c and 7d) has a similar impact as high sedimentation rates during low sea levels.

The main objective for drilling at Site U1517 was to understand whether gas hydrate dynamics contribute to the creeping behavior of the TLC. Drilling results show that the top of gas hydrate occurrence at Site U1517 (100 mbsf) is much deeper than the bottom of the TLC (66.6 mbsf) and the inferred active decollement within it (37 mbsf; Figure 1). The mechanical behavior of the landslide is therefore not associated with the occurrence of hydrates within the landslide debris, or at its base (Pecher et al., 2019). Gas migration from the BGHS toward the base of landslides (via fractures or chimneys) has been proposed to be a process contributing to slope instability at the TLC (Gross et al., 2018) and elsewhere (Elger et al., 2018). In this study, the dominant driver for methane dissociation appears to be sedimentation burying hydrate below the BGHS. The recent formation of methane hydrate evidenced by the high-chloride anomaly at Site U1517 implies that the methane released during this dissociation is at least partially offset by hydrate formation at shallower depths, reducing upward migration of methane into the TLC. It is important to note that these simulations focus only on diffusive processes; geophysical results indicate gas accumulation along vertical discontinuities in the TLC, suggesting that fluid and gas advection may be active (Gross et al., 2018).

Simulation results provide insight beyond Site U1517 and the Hikurangi Margin. Various studies have postulated gas hydrate dissociation following the LGM with consequences that include methane release to the ocean and widespread slope failure driven by gas-induced overpressure and/or sediment weakening as gas hydrate dissociates. Locations such as Site U1517, which lie close to the upper edge of gas hydrate stability, have the potential for gas hydrate to occur at shallow depths and thus could be considered a prime candidate to test changes in gas hydrate dynamics following the LGM. However, glacial cooling of bottom water will have the strongest effect in locations with a shallow BGHS, because the changes in BWT can reach the BGHS more quickly at shallow depths.

Globally, seawater cooling is expected to have been widespread at the LGM. Proxies suggest that LGM sea surface temperatures were 1–3 °C cooler at low latitudes and 3–6 °C cooler at higher latitudes (Clark et al., 2012). Although less information exists for intermediate and deep BWT, inferences from proxies (e.g., Adkins et al., 2002) and from modeling (e.g., Zhuang & Giardino, 2012) indicate that cooling is common. As a result, glacial BWT cooling lessens the likelihood of global-scale dissociation of methane

hydrate at the LGM. These results are in agreement with the majority of the literature based on analyses of sediment records and consistent with observations that there is no methane hydrate signal in atmospheric records of rapid warming preserved in ice cores (Sowers, 2006). We note that our simulations assumed temperature changes correlated to sea level changes; offsets in timing of BWT cooling relative to sea level change could impact these conclusions.

Although cooler BWT during the LGM is expected to be prevalent, warmer LGM temperatures have been suggested for some locations. For example, Portilho-Ramos et al. (2018) describe evidence from foraminiferal stable carbon isotopes that suggests methane hydrate dissociated offshore of Brazil during the LGM. At this location, changes in currents caused warming of bottom water by an estimated 4 °C during the LGM (Portilho-Ramos et al., 2018). In the Arctic Ocean, ~2 °C warmer temperatures are inferred for 1,000- to 2,500-m depth in the Arctic Ocean during the LGM based on Mg/Ca and Sr/Ca values of ostracods (Cronin et al., 2012). In locations such as these, sea level and BWT changes would both contribute to upward shifting of the BGHS at the LGM. As a result, these areas could experience LGM-related methane hydrate dissociation and possible related slope failures and/or methane release.

Finally, the simulations demonstrate that sedimentation has the potential to dominate hydrate dynamics at some margins. Based on the simulations, the effect of sedimentation appears to become negligible at 0.1 mm/year. Long-term sedimentation rates exceeding this threshold are generally in continental margin areas affected by major rivers, glaciation, or upwelling zones (Dutkiewicz et al., 2017). Short-term high sedimentation rates, such as due to glacial erosion or mass movement, would also impact hydrate dynamics, and the timing of sedimentation pulses can result in very complex histories in hydrate stability.

7. Conclusions

We illustrate how the combination of conditions of bottom water temperature, sea level changes, and sedimentation control gas hydrate dynamics offshore New Zealand, with implications that can be extrapolated to other margins. By itself, a lowering of glacial sea level followed by a postglacial rise allows methane hydrate dissociation followed by hydrate formation; however, BWT cooling/warming of 2 °C during glaciation/deglaciation can counteract the impacts of sea level change. If BWT at Site U1517 cooled by 2 °C during the LGM, sedimentation appears to be the largest factor in allowing methane hydrate formation and producing a broad high in chloride concentration. Similar processes would be expected at other margins with high (>0.1 mm/year) sedimentation rates, such as the Gulf of Mexico (Nole et al., 2018). These results reveal that perturbations of the BGHS in high-sedimentation margins may be more dependent on variations in sedimentation rate than sea level change during glacial cycles. Exceptions could occur on margins where BWT is higher during the LGM due to shifts in circulation. At these locations, the LGM could be a time of methane destabilization, slope failure, and possible methane release.

Acknowledgments
This research used samples and data provided by the International Ocean Discovery Program (IODP). We thank the scientific parties, technical staff, and crews of IODP Expeditions 372 and 375. An anonymous reviewer and Alberto Malinverno provided recommendations that greatly improved this manuscript. Shipboard data are available from the IODP database (http://iodp.tamu.edu/database/) and the strontium results are provided in Table S1. Funding for this research was provided by U.S. Science Support Program Post Expedition Activity awards to Screaton and Torres. Torres also acknowledges funding from NSF Grant OCE-1753665. Mountjoy received funding through Royal Society of New Zealand Marsden Fund Grant NIW1603 and NIWA SSIF funding in the Coasts and Oceans Programme. Heeschen acknowledges support from Deutsche Forschungsgemeinschaft (DFG).

References

Adkins, J. F., McIntyre, K., & Schrag, D. P. (2002). The salinity, temperature, and $\delta^{18}O$ of the Glacial Deep Ocean. *Science*, *298*(5599), 1769–1773. https://doi.org/10.1126/science.1076252

Bangs, N. L. B., Musgrave, R. J., & Tréhu, A. M. (2005). Upward shifts in the southern Hydrate Ridge gas hydrate stability zone following postglacial warming, offshore Oregon. *Journal of Geophysical Research*, *110*, B03102. https://doi.org/10.1029/2004JB003293

Bhatnagar, G., Chatterjee, S., Chapman, W. G., Dugan, B., Dickens, G. R., & Hirasaki, G. J. (2011). Analytical theory relating the depth of the sulfate-methane transition to gas hydrate distribution and saturation. *Geochemistry, Geophysics, Geosystems*, *12*, Q03003. https://doi.org/10.1029/2010GC003397

Boudreau, B. P. (1996). The diffusive tortuosity of fine-grained unlithified sediments. *Geochimica et Cosmochimica Acta*, *60*, 3139–3142. https://doi.org/10.1016/0016-7037(96)00158-5

Carpenter, G. (1981). Coincident sediment slump/clathrate complexes on the U.S. Atlantic continental slope. *Geo-Marine Letters*, *1*, 29. https://doi.org/10.1007/BF02463298

Carter, L., & Manighetti, B. (2006). Glacial/interglacial control of terrigenous and biogenic fluxes in the deep ocean off a high input, collisional margin: A 139 kyr-record from New Zealand. *Marine Geology*, *226*(3-4), 307–322.

Carter, L., Manighetti, B., Ganssen, G., & Northcote, L. (2008). Southwest pacific modulation of abrupt climate change during the Antarctic Cold Reversal-Younger Dryas. *Palaeogeography Palaeoclimatology Palaeoecology*, *260*, 284–298.

Clark, P. U., Shakun, J. D., Baker, P. A., Bartlein, P. J., Brewer, S., Brook, E., et al. (2012). Global climate evolution during the last deglaciation. *Proceedings of the National Academy of Sciences*, *109*(19), E1134–E1142. https://doi.org/10.1073/pnas.1116619109

Claypool, G. E., & Kaplan, I. R. (1974). The origin and distribution of methane in marine sediments. In I. R. Kaplan (Ed.), *Natural gases in marine sediments* (pp. 99–139). New York: Plenum.

Cronin, T. M., Dwyer, G. S., Farmer, J., Bauch, H. A., Spielhagen, R. F., Jakobsson, M., et al. (2012). Deep Arctic Ocean warming during the last glacial cycle. *Nature Geoscience*, *5*(9), 631–634. https://doi.org/10.1038/ngeo1557

Daigle, H., & Dugan, B. (2014). Pore size controls on the base of the methane hydrate stability zone in the Kumano Basin, offshore Japan. *Geophysical Research Letters*, *41*, 8021–8028. https://doi.org/10.1002/2014GL062135

Dickens, G. R., & Quinby-Hunt, M. S. (1994). Methane hydrate stability in seawater. *Geophysical Research Letters*, *21*, 2115–2118. https://doi.org/10.1029/94GL01858

Dutkiewicz, A., Müller, R. D., Wang, X., O'Callaghan, S., Cannon, J., & Wright, N. M. (2017). Predicting sediment thickness on vanished ocean crust since 200 Ma. *Geochemistry, Geophysics, Geosystems*, *18*, 4586–4603. https://doi.org/10.1002/2017GC007258

Elger, J., Berndt, C., Rüpke, L., Krastel, S., Gross, F., & Geissler, W. H. (2018). Submarine slope failures due to pipe structure formation. *Nature Communications*, *9*(1), 715. https://doi.org/10.1038/s41467-018-03176-1

Faure, K., Greinert, J., von Deimling, J. S., McGinnis, D. F., Kipfer, R., & Linke, P. (2010). Methane seepage along the Hikurangi Margin of New Zealand: Geochemical and physical data from the water column, sea surface and atmosphere. *Marine Geology*. https://doi.org/10.1016/j.margeo.2010.01.001

Gross, F., Mountjoy, J. J., Crutchley, G. J., Böttner, C., Koch, S., Bialas, J., et al. (2018). Free gas distribution and basal shear zone development in a subaqueous landslide—Insight from 3D seismic imaging of the Tuaheni Landslide Complex, New Zealand. *Earth and Planetary Science Letters*, *502*, 231–243. https://doi.org/10.1016/j.epsl.2018.09.002

Haeckel, M., Suess, E., Wallmann, K., & Rickert, D. (2004). Rising methane gas bubbles form massive hydrate layers at the seafloor. *Geochimica et Cosmochimica Acta*, *68*, 4335–4345. https://doi.org/10.1016/j.gca.2004.01.018

Henrich, R., Hanebuth, T. J. J., Krastel, S., Neubert, N., & Wynn, R. B. (2008). Architecture and sediment dynamics of the Mauritania slide complex. *Marine and Petroleum Geology*, *25*(1), 17–33. https://doi.org/10.1016/j.marpetgeo.2007.05.008

Hornbach, M. J., Lavier, L. L., & Ruppel, C. D. (2007). Triggering mechanism and tsunamogenic potential of the Cape Fear Slide complex, U. S. Atlantic margin. *Geochemistry, Geophysics, Geosystems*, *8*, Q12008. https://doi.org/10.1029/2007GC001722

Huhn, K. (2016). DSRV Sonne SO247 Cruise Report—SlamZ: Slide activity on the Hikurangi margin, New Zealand, Wellington–Auckland, 27 March– 27 April 2016. Bundesministerium für Bildung und Forschung. https://www.portal-forschungsschiffe.de/lw_resource/datapool/_items/item_183/fahrtbericht_so247.pdf

Karstens, J., Haflidason, H., Becker, L. W., Berndt, C., Rüpke, L., Planke, S., et al. (2018). Glacigenic sedimentation pulses triggered post-glacial gas hydrate dissociation. *Nature Communications*, *9*(1), 635. https://doi.org/10.1038/s41467-018-03043-z

Kastner, M., Solomon, E. A., Harris, R. N., & Torres, M. E. (2014). Fluid origins, thermal regimes, and fluid and solute fluxes in the forearc of subduction zones. In R. Stein, D. K. Blackman, F. Inagaki, & H. Larsen (Eds.), *Developments in Marine Geology* (Vol. 7, pp. 671–733). Amsterdam: Elsevier. https://doi.org/10.1016/B978-0-444-62617-2.00022-0

Kennett, J. P., Cannariato, K. G., Hendy, I. L., & Behl, R. J. (2003). Methane hydrates in Quaternary climate change: The clathrate gun hypothesis. In J. P. Kennett, K. G. Cannariato, I. L. Hendy, & R. J. Behl (Eds.), *Methane Hydrates in Quaternary Climate Change: The Clathrate Gun Hypothesis* (pp. 1–9). Washington, DC: American Geophysical Union. https://doi.org/10.1002/9781118665138.ch0

Kim, J.-H., Torres, M. E., Hong, W.-L., Choi, J., Riedel, M., Bahk, J.-J., & Kim, S.-H. (2013). Pore fluid chemistry from the second gas hydrate drilling expedition in the Ulleung Basin (UBGH2): Source, mechanisms and consequences of fluid freshening in the central part of the Ulleung Basin, East Sea. *Marine and Petroleum Geology*, *47*, 99–112. https://doi.org/10.1016/j.marpetgeo.2012.12.011

Kuhlmann, J., Orpin, A. R., Mountjoy, J. J., Crutchley, G. J., Henrys, S., Lunenburg, R., & Huhn, K. (2018). Seismic and lithofacies characterization of a gravity core transect down the submarine Tuaheni Landslide Complex, NE New Zealand. *Geological Society, London, Special Publications*, *477*, SP477–SP437.

Li, A., Davies, R. J., & Mathias, S. (2017). Methane hydrate recycling offshore of Mauritania probably after the last glacial maximum. *Marine and Petroleum Geology*, *84*, 323–331. https://doi.org/10.1016/j.marpetgeo.2017.04.007

Malinverno, A. (2010). Marine gas hydrates in thin sand layers that soak up microbial methane. *Earth and Planetary Science Letters*, *292*, 399–408. https://doi.org/10.1016/j.epsl.2010.1002.1008

Malinverno, A., Cook, A. E., Daigle, H., & Oryan, B. (2018). Glacial cycles influence marine methane hydrate formation. *Geophysical Research Letters*, *45*, 724–732. https://doi.org/10.1002/2017GL075848

Malinverno, A., Kastner, M., Torres, M. E., & Wortmann, U. G. (2008). Gas hydrate occurrence from pore water chlorinity and downhole logs in a transect across the northern Cascadia margin (Integrated Ocean Drilling Program Expedition 311). *Journal of Geophysical Research*, *113*, B08103. https://doi.org/10.01029/02008JB005702

McCarthy, M., Zirkle, B., Torres, M. E., & Haley, B. A. (2018). Data report: $^{87}Sr/^{86}Sr$ in pore fluids from Expedition 362. In *Proceedings of the International Ocean Discovery Program* (Vol. 362). College Station, TX: International Ocean Discovery Program. https://doi.org/10.14379/iodp.proc.362.201.2018

Mestdagh, T., Poort, J., & De Batist, M. (2017). The sensitivity of gas hydrate reservoirs to climate change: Perspectives from a new combined model for permafrost-related and marine settings. *Earth-Science Reviews*, *169*, 104–131. https://doi.org/10.1016/j.earscirev.2017.04.013

Mountjoy, J. J., Pecher, I., Henrys, S., Crutchley, G., Barnes, P. M., & Plaza-Faverola, A. (2014). Shallow methane hydrate system controls ongoing, downslope sediment transport in a low-velocity active submarine landslide complex, Hikurangi Margin, New Zealand. *Geochemistry, Geophysics, Geosystems*, *15*, 4137–4156. https://doi.org/10.1002/2014GC005379

Murray, N. A., McManus, J., Palmer, M. R., Haley, B., & Manners, H. (2018). Diagenesis in tephra-rich sediments from the Lesser Antilles Volcanic Arc: Pore fluid constraints. *Geochimica et Cosmochimica Acta*, *228*, 119–135.

Nole, M., Daigle, H., Cook, A. E., Malinverno, A., & Flemings, P. B. (2018). Burial-driven methane recycling in marine gas hydrate systems. *Earth and Planetary Science Letters*, *499*, 197–204. https://doi.org/10.1016/j.epsl.2018.07.036

O'Regan, M., & Moran, K. (2010). Deep water methane hydrates in the Arctic Ocean: Reassessing the significance of a shallow BSR on the Lomonosov Ridge. *Journal of Geophysical Research*, *115*, B05102. https://doi.org/10.1029/2009JB006820

Paull, C. K., Ussler, W., & Borowski, W. S. (1994). Sources of biogenic methane to form marine gas hydrates: In situ production or upward migration? *Annals of the New York Academy of Sciences*, *715*, 392–409. https://doi.org/10.1111/j.1749-6632.1994.tb38852.x

Paull, C. K., Ussler, W., & Dillon, W. P. (1991). Is the extent of glaciation limited by marine gas hydrates? *Geophysical Research Letters*, *18*(3), 432–434. https://doi.org/10.1029/91GL00351

Paytan, A., Kastner, M., Martin, E. E., Macdougall, J. D., & Herbert, T. (1993). Marine barite as a monitor of seawater strontium isotope composition. *Nature*, *366*(6454), 445.

Pecher, I. A., Barnes, P. M., LeVay, L. J., & the Expedition 372 Scientists (2019). Creeping gas hydrate slides. In *Proceedings of the International Ocean Discovery Program* (Vol. 372A). College Station, TX: International Ocean Discovery Program. https://doi.org/10.14379/iodp.proc.372A.2019

Pecher, I. A., Villinger, H., Kaul, N., Crutchley, G. J., Mountjoy, J. J., Huhn, K., et al. (2017). A fluid pulse on the Hikurangi subduction margin: Evidence from a heat flux transect across the upper limit of gas hydrate stability. *Geophysical Research Letters*, *44*, 12,385–12,395. https://doi.org/10.1002/2017GL076368

Peizhen, Z., Molnar, P., & Downs, W. R. (2001). Increased sedimentation rates and grain sizes 2–4 Myr ago due to the influence of climate change on erosion rates. *Nature*, *410*(6831), 891.

Portilho-Ramos, R. C., Cruz, A. P., Barbosa, C. F., Rathburn, A. E., Mulitza, S., Venancio, I. M., et al. (2018). Methane release from the southern Brazilian margin during the last glacial. *Scientific Reports*, *8*(1), 5948. https://doi.org/10.1038/s41598-018-24420-0

Riedel, M., Collett, T., Malone, M., Akiba, F., Blanc-Valleron, M., Ellis, M., et al. (2006). Gas hydrate transect across Northern Cascadia Margin. *Eos, Transactions American Geophysical Union*, *87*(33), 325, 330, and 332. https://doi.org/10.1029/2006EO330002

Ross, N., Torres, M. E., Haley, B. A., Solomon, E. A., & Kastner, M. (2015). Data report: Strontium isotope analyses of pore fluids from the CRISP-A transect drilled during Expeditions 334 and 344. In *Proceedings of the International Ocean Discovery Program* (Vol. 344). College Station, TX: International Ocean Discovery Program. https://doi.org/10.2204/iodp.proc.344.201.2015

Ruppel, C. D., & Kessler, J. D. (2017). The interaction of climate change and methane hydrates. *Reviews of Geophysics*, *55*, 126–168. https://doi.org/10.1002/2016RG000534

Sample, J. C., Torres, M. E., Fisher, A., Hong, W. L., Destrigneville, C., Defliese, W. F., & Tripati, A. E. (2017). Geochemical constraints on the temperature and timing of carbonate formation and lithification in the Nankai Trough, NanTroSEIZE transect. *Geochimica et Cosmochimica Acta*, *198*, 92–114.

Sloan, E. D. (1998). *Clathrate hydrates of natural gases* (2nd ed.). New York: Marcel Dekker.

Solomon, E. A., Spivack, A. J., Kastner, M., Torres, M. E., & Robertson, G. (2014). Gas hydrate distribution and carbon sequestration through coupled microbial methanogenesis and silicate weathering in the Krishna-Godavari Basin, offshore India. *Marine and Petroleum Geology*, *58*, 233–253.

Sowers, T. (2006). Late Quaternary atmospheric CH_4 isotope record suggests marine clathrates are stable. *Science*, *311*(5762), 838–840. https://doi.org/10.1126/science.1121235

Sultan, N., Cochonat, P., Foucher, J.-P., & Mienert, J. (2004). Effect of gas hydrates melting on seafloor slope instability. *Marine Geology*, *213*(1-4), 379–401. https://doi.org/10.1016/j.margeo.2004.10.015

Teichert, B. M. A., Torres, M. E., Bohrmann, G., & Eisenhauer, A. (2005). Fluid sources, fluid pathways and diagenetic reactions across an accretionary prism revealed by Sr and B geochemistry. *Earth and Planetary Science Letters*, *239*(1–2), 106–121. https://doi.org/10.1016/j.epsl.2005.08.002

Torres, M. E., Cox, T., Hong, W. L., McManus, J., Sample, J. C., Destrigneville, C., et al. (2015). Crustal fluid and ash alteration impacts on the biosphere of Shikoku Basin sediments, Nankai Trough, Japan. *Geobiology*, *13*(6), 562–580. https://doi.org/10.1111/gbi.12146

Torres, M.E., Kim, J-H., Choi, J., Ryu, J-B, Bahk, J-J, Riedel, M., et al. (2011). Occurrence of high salinity fluids associated with massive near-seafloor gas hydrate deposits. In: *Proceedings of the 7th International Conference on Gas Hydrates* (ICGH 2011), Edinburgh, Scotland, United Kingdom, July 17-21, 2011.

Torres, M. E., Trehu, A. M., Cespedes, N., Kastner, M., Wortmann, U. G., Kim, J.-H., et al. (2008). Methane hydrate formation in turbidite sediments of northern Cascadia, IODP Expedition 311. *Earth and Planetary Science Letters*, *271*(1-4), 170–180. https://doi.org/10.1016/j.epsl.2008.03.061

Torres, M. E., Wallmann, K., Trehu, A. M., Bohrmann, G., Borowski, W. S., & Tomaru, H. (2004). Gas hydrate growth, methane transport, and chloride enrichment at the southern summit of Hydrate Ridge, Cascadia margin off Oregon. *Earth and Planetary Science Letters*, *226*, 225–241.

Tréhu, A. M., Long, P. E., Torres, M. E., Bohrmann, G., Rack, F. R., Collett, T. S., et al. (2004). Three-dimensional distribution of gas hydrate beneath the seafloor: Constraints from ODP Leg 204. *Earth and Planetary Science Letters*, *222*(3-4), 845–862. https://doi.org/10.1016/j.epsl.2004.03.035

Ussler, W., & Paull, C. K. (2001). Ion exclusion associated with marine gas hydrate deposits. In C. K. Paull, & W. P. Dillon (Eds.), *Natural gas hydrates: Occurrence, distribution, and detection*, *Geophysical Monographs* (Vol. 124, pp. 41–51). Washington, D. C: American Geophysical Union.

Waelbroeck, C., Labeyrie, L., Michel, E., Duplessy, J. C., McManus, J. F., Lambeck, K., et al. (2002). Sea-level and deep water temperature changes derived from benthic foraminifera isotopic records. *Quaternary Science Reviews*, *21*(1-3), 295–305. https://doi.org/10.1016/S0277-3791(01)00101-9

Wallmann, K., Pinero, E., Burwicz, E., Haeckel, M., Hensen, C., Dale, A., & Ruepke, L. (2012). The global inventory of methane hydrate in marine sediments: A theoretical approach. *Energies*, *5*(7), 2449–2498. https://doi.org/10.3390/en5072449

Wallmann, K., Riedel, M., Hong, W. L., Patton, H., Hubbard, A., Pape, T., et al. (2018). Gas hydrate dissociation off Svalbard induced by isostatic rebound rather than global warming. *Nature Communications*, *9*(1), 83. https://doi.org/10.1038/s41467-017-02550-9

Wei, W., Kastner, M., & Spivack, A. (2008). Chlorine stable isotopes and halogen concentrations in convergent margins with implications for the Cl isotopes cycle in the ocean. *Earth and Planetary Science Letters*, *266*, 90–104.

Zhuang, K., & Giardino, J. R. (2012). Ocean cooling pattern at the last glacial maximum. *Advances in Meteorology*. https://doi.org/10.1155/2012/213743